Prepared for
AIAA Journal

[redacted]

CALCULATED TEMPERATURE HISTORIES OF VAPORIZING DROPLETS TO THE CRITICAL POINT

By Paul R. Wieber[1]

Lewis Research Center
National Aeronautics and Space Administration
Cleveland, Ohio

ABSTRACT

Digital computations of droplet steady-state temperatures and droplet mass and temperature histories were made to determine if droplet temperatures could approach the critical point. Pressures to 2000 psia were investigated. At sufficiently high pressure, the calculations showed both heptane and oxygen droplets heating to their respective critical temperatures. With increasing total pressure, a reduction occurred in both the downstream distance after injection and the mass evaporated before the droplets reached the critical point. This implied that a vaporization model may be inadequate in describing overall combustion rates at high total pressures. Rapid droplet heating rates indicated that droplets could approach the critical point during combustion instability at high pressures. This phenomenon could thus be involved in a mechanism for high-pressure combustion instability.

SUMMARY

Droplet equilibrium temperatures and histories of droplet temperatures, evaporation rates, and trajectories at rocket-combustor conditions were computed to determine the conditions required for heptane and oxygen droplets to attain their critical temperatures. At sufficiently high total gas

[1]Aero-Space Technologist

pressures, solutions of droplet equilibrium temperatures could not be obtained, and calculated histories at these high pressures showed droplets heating to the critical point. Considerations of the physical rates that establish droplet thermal equilibrium offered an explanation for the trends in the computed droplet steady-state temperatures and illustrated the process by which droplets attain the critical point. In droplet histories at high gas pressures, as little as 1/2 percent of the initial mass of an oxygen droplet was vaporized before the droplet reached the critical point, whereas at lower pressures all of the droplet mass was evaporated in the vaporization process without the droplet achieving the critical point. The results of the computations indicated that the vaporization model may not be valid for use in the design of high-pressure rocket combustors. Application of the results to combustion instability at high pressures indicated that the pressure perturbations or gas velocity perturbations, which are associated with combustion instability, could cause temperatures of all but the largest droplets to approach the critical point. This phenomenon could cause the formation of masses of vapor for diffusion into the bulk gas stream and should be considered in any high-pressure combustion-instability mechanism. Liquid oxygen vaporization rates also appeared to be potentially sensitive to small pressure perturbations and could be important in the initiation of combustion instability.

INTRODUCTION

In the operation of a liquid-propellant rocket engine, the rate-controlling process has been shown, in many cases, to be the vaporization

of propellant droplets formed soon after injection (ref. 1). The evaporation process includes a period in which the droplet is heated from its injection temperature to a steady-state (equilibrium) temperature that is characterized by the transformation of all heat reaching the droplet surface into latent heat of vaporization with no further contribution to sensible heating of the liquid. The initial heating period has been shown to be an appreciable part of droplet life (e.g., refs. 2 to 5). These studies also indicate that the droplet equilibrium temperature increases with increasing gas temperature and pressure and perhaps approaches the critical temperature of the liquid.

This report presents calculations of steady-state temperatures and temperature, mass, and trajectory histories of droplets in high-pressure and high-temperature environments. The calculations were made to determine under what conditions the critical point is reached by vaporizing drops. Mass transfer above critical conditions cannot be calculated because of the lack of theory for this region. Thus, an upper limit on the regime in which the present vaporization theory may be applied is defined herein.

The propellants studied were liquid heptane and liquid oxygen. The boundary conditions for the calculations were representative of those occurring in the high-intensity combustion fields that exist in rocket engines. Total gas pressures up to 2000 psi were investigated. The results of the calculations are presented graphically. Calculated temperatures show that the droplets approach the critical condition before vaporization is completed. The significance of this phenomenon to combustor design and to combustion-instability mechanisms is discussed.

THEORY

A detailed theoretical analysis of heat transfer to the surface of an evaporating droplet may be found in references 2 and 4. References 4 and 6 contain detailed derivations of the equations used for the calculations reported herein. Accordingly, only a brief description of the droplet model with the final equations is presented.

The droplet is surrounded by a vapor film. Heat transferred into this film from the high-temperature environment serves to superheat the exuding vapor and to provide a heat flux at the liquid surface of the droplet. This surface heat flux raises the droplet temperature and provides enthalpy for vaporization. The assumption of effectively infinite liquid thermal conductivity is made implying existence of a uniform droplet temperature. The assumption is based on rapid internal circulation within the droplet. Reference 3 shows evidence for this circulation. A heat balance around the drop leads to the following expression for the rate of change of droplet temperature with time:

$$\frac{dT_L}{dt} = \frac{3}{2C_{p,L}\rho_L r^2}\left\{k_m(T_T - T_L)\frac{z}{e^z - 1}(2 + 0.6\ Pr^{1/3}Re^{1/2}) - \frac{D_V M_L H_V}{R}\frac{P_T}{T_m}\left[\ln\left(\frac{P_T}{P_T - P_L}\right)\right](2 + 0.6\ Sc^{1/3}Re^{1/2})\right\} \quad (1)$$

where

$$z = \frac{D_V M_L C_{p,V}}{k_m R}\frac{P_T}{T_m}\left[\ln\left(\frac{P_T}{P_T - P_L}\right)\right]\left(\frac{2 + 0.6\ Sc^{1/3}Re^{1/2}}{2 + 0.6\ Pr^{1/3}Re^{1/2}}\right)$$

The mass evaporation rate in reference 4 can be related to the rate of change of radius with time, if the droplet is assumed to be spherical:

$$\frac{dW}{dt} = \left(12.5564\rho_L r^2 \frac{dr}{dt} + 4.1888r^3 \frac{d\rho_L}{dt}\right)$$

$$= 6.2832 \frac{D_v M_L r}{R} \frac{P_T}{T_m}\left[\ln\left(\frac{P_T}{P_T - P_L}\right)\right]\left(2 + 0.6\ Sc^{1/3}Re^{1/2}\right) \qquad (2)$$

Consideration of the aerodynamic forces on a liquid sphere and use of an empirical expression for drag coefficient gives the following equation for droplet acceleration in the combustor:

$$\frac{dU_d}{dt} = 5.656 \frac{\rho_m^{0.16}\mu_m^{0.84}}{\rho_L r^{1.84}} (U - U_d)^{1.16} \qquad (3)$$

Finally, the combustion gas velocity is assumed to be proportional to the total amount of mass evaporated from the drop:

$$U = U_F(1 - W/W_o) \qquad (4)$$

These equations were used to calculate vaporization histories for a droplet in rocket-engine conditions. The heptane calculations were made by solving equation (2) for dr/dt and by using the resulting expression to describe the mass-transfer rate. Later modifications utilized dW/dt in the oxygen calculations.

The major variables investigated were drop sizes of 10, 100, and 1000 microns and gas pressures from 100 to 2000 psia. Although vaporization histories have previously been computed for rocket-engine conditions, (e.g., refs. 6 and 7), chamber pressures did not exceed 600 psia. The remaining conditions used to specify the rocket combustor were: final gas velocity, 800 ft/sec; gas temperature, 5000° R; droplet injection velocity, 80 ft/sec; droplet injection temperatures, 650° R for heptane and 140° R for liquid oxygen.

The steady-state condition can be calculated by setting equation (1), which describes droplet heating, equal to zero, (as in ref. 4). The result is the following equation for droplet equilibrium temperature:

$$T_{L,E} = T_T - \frac{H_V}{C_{p,v}} \left(e^z - 1\right) \tag{5}$$

Thus, the equilibrium temperature is dependent on the gas temperature and pressure, the physical properties that can be a function of both the liquid temperature and gas conditions, and the product of the drop size and the drop velocity relative to the gas, included in the Reynolds number. For this reason a trial-and-error solution of the equation was necessary. Boundary conditions for this calculation included gas pressures from 50 to 1000 psia, gas temperatures from 4000° to 6000° R, and Reynolds numbers from zero to infinity.

Solution of the droplet-history and equilibrium-temperature equations was performed on the Lewis Research Center IBM 7090 digital computer. The mass (or radius), temperature, and drop velocity of the vaporization-history equations were obtained by use of the Runge-Kutta integration technique. The gas velocity and all physical properties were calculated directly at each trial value of the above three variables. Termination of each history computation occurred when either the liquid temperature exceeded the critical temperature or 96 percent of the initial droplet mass was evaporated. The latter end point was arbitrarily chosen because the differentials become unbounded as drop radius approaches zero. A check of this program was made by running a case specified in reference 6. A

comparison with the results of that reference showed satisfactory agreement. A program that involves converging trials with equation (5) gave the equilibrium temperature to the nearest hundredth degree.

The physical properties were calculated in subroutines for flexibility. The density, heat of vaporization, and vapor pressure of the liquid were obtained directly from data of reference 8 for heptane and references 9 to 13 for oxygen. Most of the other physical properties are summarized in the appendix of reference 6 in the form of linear and quadratic equations, and the relations for calculation of mean property values are also described. However, it was necessary to determine new equations for the specific heat, thermal conductivity, diffusivity, and viscosity of water vapor. The gas was treated as a polar molecule, and the methods in reference 14 with some corrected tables and calculations from reference 15 were employed to calculate these physical properties. Equations were fitted to the results and are listed in appendix A.

RESULTS AND DISCUSSION

Initial calculation of some vaporization histories showed that the droplet temperature did not attain equilibrium at high pressure but instead continued rising to the critical point. Since the primary variable was liquid temperature, a study of the variation of equilibrium temperature with 'changing' chamber parameters was made before continuing with the droplet-history computations. The results are shown in figure 1 as reduced temperatures, $T_{L,E}/T_{crit}$. They are plotted against the total gas pressure P_T and also the ratio of the total pressure to the critical pressure of the liquid, P_T/P_{crit}, (reduced total pressure). Figure 1 shows

that heptane requires a reduced total pressure from 1.78 to 2.30 for attainment of its critical point, depending on the value of $r \Delta V$, the product of the drop size and the velocity of the drop relative to the gas. The sensitivity of equilibrium temperature to $r \Delta V$ increases with increasing liquid temperature. There is a region for heptane just below the critical temperature in which no solution of equilibrium temperatures exists. In contrast, oxygen reaches its critical point at a reduced total pressure of unity, and its equilibrium temperature is independent of $r \Delta V$. The curve of oxygen equilibrium temperatures extends essentially to the critical temperatures. The trends displayed in figure 1 and the appearance of the critical-heating phenomenon can be explained by considerations of the heat- and mass-transfer rates at the droplet surface. These considerations are presented in appendix B.

The equilibrium temperatures of oxygen presented herein are somewhat higher than those computed in reference 6 for liquid oxygen with gaseous heptane. This is due mainly to use of a higher value for gas thermal conductivity in this paper. Gas properties were calculated herein with water vapor treated as a polar molecule. As a check, a linear extrapolation to 1800° R of experimental data for water vapor (refs. 16 and 17) gave a value of thermal conductivity very close to that calculated from the curve fit used in this study. These higher oxygen temperatures are significant because they have vapor pressures associated with them that are almost equal to the respective chamber pressures. This indicates that the vaporization of oxygen droplets may possibly take place through surface ebullition. If this is so, a small pressure rarefaction interacting with

the droplet could produce violent boiling that might shatter the drop or, at least, release a surge of oxygen vapor. This phenomenon might be important in initiation and support of combustion instability in combustors that employ liquid oxygen.

The calculations of equilibrium temperatures discussed previously determined the gas conditions that are required for a droplet to reach its critical point. These conditions may be found in high-pressure combustors such as rocket and diesel engines. In fact, droplet-history calculations for diesel-engine conditions have indicated that liquid temperatures reach the critical temperature (ref. 18). The examples of thermodynamic and trajectory histories presented in figures 2 and 3 illustrate the rates of heating of the droplets and allow some estimate to be made of the importance of this phenomenon in a rocket-combustion model. Figures 2(a) and (b) show histories for a 100-micron-radius heptane droplet vaporizing in a simulated rocket combustor, which operates at a chamber pressure of 1000 psia. Both plots have the time after injection and the distance downstream from the injector plotted on the abscissa. Figure 2(a) shows droplet temperature and evaporation rate as ordinates. Up to about 1 millisecond, the droplet behavior is similar to low pressure histories; however, the droplet continues heating to the critical point with a simultaneous rapid rise in vaporization rate. Figure 2(b) shows that the fraction of the initial drop weight still remaining at the critical point is about 0.79. The droplet radius increases rapidly near the critical point as a result of the rapidly decreasing liquid density and despite the high vaporization rate. Figures 3(a) and (b) depict the same parameters

for a 100-micron-radius oxygen droplet under identical boundary conditions as heptane in figure 2 except for injection temperature. The trends are the same as for heptane but more severe in this case. The droplet reaches the critical point very rapidly, even before the gas velocity has equaled the droplet velocity. Less than 2 percent of the initial droplet mass has evaporated at this time.

The results of all the droplet-history calculations are expressed in figures 4 and 5. Figure 4 shows either the downstream distance where 96 percent of the droplet initial mass is vaporized or the location where the critical point is reached, whichever occurs first, against total and reduced total pressures. These distances are normalized for more convenient plotting by dividing by the corresponding distance calculated for a total gas pressure of 100 psia, x_{100}. Values of x_{100} are listed in the table in the figure. The curves in the region from A to B show the lengths required to vaporize 96 percent of the initial droplet mass. The initial slopes of the curves from A to B indicate the reduction in vaporization length due to enhancement of the evaporation process by increasing pressure. In the region of B, there is a marked increase in slope, especially for the oxygen curves. This indicates that the critical temperature is being approached by the droplets, and the curves from B to D show the length required to reach the critical point. The second inflection in the heptane curves at C occurs because the droplets have achieved the critical temperature before the relative velocity between gas and drop has reached zero. The thickness of the shaded region shows the distance spread for drops of 10, 100, and 1000 microns initial radii.

Heptane shows a sensitivity to drop size below the point B. This sensitivity is due to the dependency of heptane droplet equilibrium temperature on $r\,\Delta V$ as indicated by figure 1.

Figure 5 indicates the variation with total and reduced total pressures of the percent weight evaporated before the critical point is reached. When the total gas pressure equals the critical pressure, the oxygen curves show that only 5 percent of the droplet mass was evaporated before the critical temperature was reached. All curves are essentially independent of initial droplet size.

These history calculations indicate that droplets evaporating in rocket-engine conditions at high chamber pressures will achieve the critical point at relatively short chamber lengths before an appreciable amount of mass is evaporated. Accordingly, it must be concluded that the vaporization model describes only a initial part of liquid-propellant combustion under high pressure. When the critical point is reached, the liquid interface vanishes. Diffusion of the propellant vapor into the gaseous environment might then be the rate-controlling step of the combustion process in the supercritical regime. Combustor design for high pressures should include the possibility of a change in the rate-controlling mechanism. Increasing the thrust level of existing hardware by raising propellant flow density could also cause droplets to enter the supercritical regime, since chamber pressure is also increased in the process.

Since the calculations have shown that liquid droplets can reach their critical temperatures, it is appropriate to reexamine some of the assumptions originally made in the derivation of the equations. It should be

emphasized that the theory used in these calculations breaks down very near the critical point. In the original derivation, unidirectional diffusion was assumed based on small regression rates of the liquid surface. These rates become higher near the critical point. The use of the empirical expressions for Nusselt numbers may be questioned, since these expressions were developed for droplets far from critical conditions. Some physical properties, especially the thermal conductivity and diffusion coefficient, are not accurately known near the critical point, and this uncertainty may affect these results. Droplet breakup was neglected, but near the critical point the surface tension of the liquid becomes very small, enhancing the possibility of breakup. The drag-coefficient expression used in the history calculations was determined for conditions far from the critical point. Nevertheless, these factors only affect the various rates involved and do not negate the possibility that the droplets can reach their critical points.

In view of the very high heating rates, a more serious assumption was that the temperature of the drop is always uniform throughout its interior due to internal mixing. Absence of this mixing suggests that only an outer "skin" of the droplet experiences the high heat fluxes, insulating the colder liquid core and allowing liquid droplets to exist at gas pressures and temperatures far above the critical conditions of the liquid. Reference 3 was cited as an observation of the internal motion required to produce a uniform droplet temperature, but the droplets in reference 3 were not surrounded by a flame front. In reference 19, it was observed that internal motion of burning droplets ceased soon after

ignition, evidently because the surrounding combustion zone isolated the droplets from the external gaseous flow field. Nonetheless, with conduction as the only heat-transfer mechanism, reference 19 indicated that drops soon acquire relatively uniform temperatures throughout their interiors as evaporation proceeds. Furthermore, the droplets in reference 19 were suspended in a natural convection field. Consideration of the severe external gas flows that droplets experience in rocket combustors and the internal liquid motion that the injection process must cause makes the existence of internal circulation seem highly probable. Heptane and oxygen have low viscosities, which makes internal fluid motion even more probable. With these considerations, the model of uniform droplet temperature due to an effectively infinite liquid thermal conductivity seems more realistic than one involving a large temperature gradient in the droplet. The former model is thus used in this paper. Only experimental measurements of internal droplet temperatures under very high incident heat fluxes and in a variety of surrounding flow fields can serve as a test of this assumption.

Thus, despite these qualifications, it seems reasonable to assume that the critical-heating phenomenon described does occur at some high pressure. At best, these calculations based on present vaporization theory yield acceleration, heating, and evaporation rates that describe droplet behavior at high pressures. At the very worst, the computations define the upper area of application of normal vaporization theory and indicate that a vaporization model cannot be used as the sole design criteria for extremely high-pressure combustors.

Critical heating of droplets may also be applicable to combustion

instability models at high pressures. Figure 1 indicates that a heptane droplet at a reduced chamber pressure of 2.0 with $r \Delta V = 10^{-4}$ could achieve an equilibrium temperature. A gas-velocity fluctuation of sufficient magnitude to increase $r \Delta V$ above 10^{-3} would induce heating of the droplet, perhaps to the critical point, with sufficient time of action. This is not the case for oxygen. Similarly, a positive pressure perturbation is reflected on figure 1 as an increase along the abscissa, and the droplet temperature increases along a line of constant $r \Delta V$ to the critical point. From an estimate of heating rates from figures 2(a) and 3(a), a 1000-cycle-per-second oscillation with a root-mean-square pressure amplitude of 150 psi would have a high-pressure half cycle of adequate action time and strength to cause droplets smaller than a 100-micron radius to heat to the critical point from their equilibrium temperature at 700 psia. Lower frequencies with increased periods make this even more probable.

The preceding conditions postulate an average chamber pressure low enough to allow the droplets to obtain an equilibrium temperature at that pressure. In this case, heating to the critical point is only possible during the high-pressure half cycle of the oscillation. On the other hand, a combustor operating at an instantaneous pressure always above the value necessary for the propellant droplets to heat to the critical point could experience this critical heating over the entire pressure cycle. Some droplets will have normal lifetimes shorter than the period of the oscillations, and more of these droplets would reach the critical point during the half cycle when the pressure and heating rates are the highest.

Both the velocity and pressure fluctuations would affect only small to medium-sized droplets. Large heptane drops greater than about 100-micron radius would already be on the curve of high $r\,\Delta V$ (fig. 1) because of the large value of r. A further increase in ΔV thus would not affect the steady-state liquid temperature. Also, a large drop of either propellant has considerable thermal inertia with lower heating rates and could not respond to an oscillating pressure wave. The pressure wave thus would tend to shift the propellant spray size distribution by the heating of small drops to the critical point. The temperature of small droplets would respond rapidly to the instantaneous pressure and would tend to reach the critical point during the high-pressure portion of each oscillation. The thermal inertia of the large drops would tend to average the fluctuating heating rate, and their temperature would be relatively unaffected over a single cycle. Since sprays generally contain a large number of small drops, overall evaporation rates could vary widely with time.

If many droplets are attaining the critical point, the mechanism for driving a wave under this condition may differ from the case where no critical heating occurs. It is pointless at this time to attempt a detailed examination of the absolute effect this critical heating phenomena might have on the combustion process. Too little is known about these processes at high pressure. The previous discussion only delineates the conditions under which the phenomena could occur and points out that a potential change in mechanism could exist in the high-pressure regime.

CONCLUSIONS

The following conclusions may be made as results of the calculations presented herein. Propellant droplets may heat to their critical points under sufficiently high gas pressures. This phenomenon defines the upper limit of application for vaporization theory in the design of high-pressure combustors, and it could be involved in combustion-instability mechanisms at high pressures. A better definition of this process requires the evolution of a new theory including equimolal counter diffusion. Some other work required to define this little-known regime involves accurate evaluation of physical properties near the critical point, studies of the effect of pressure and gas velocity perturbations on droplet evaporation rates and temperature fluctuations at high mean gas pressures, determination of temperature gradients in droplets experiencing high incident heat fluxes, and experimental verification of the existence of the critical heating phenomenon.

SYMBOLS

C_p specific heat, Btu/(lb)(^oR)

D diffusivity, ft^2/sec

H_V heat of vaporization, Btu/lb

k thermal conductivity, Btu/(ft)(sec)(^oR)

ln natural logarithm

M molecular weight, lb/lb-mole

P_L vapor pressure of liquid at droplet surface, lb/ft^2

P_T total pressure of combustion gas, lb/ft^2

Pr Prandtl Number, $(C_{p,m}\mu_m/k_m)$

R	gas constant, ft-lb/(lb-mole)(^{o}R)
Re	Reynolds number, $(2r\rho_m\|\Delta V\|/\mu_m)$
r	droplet radius, ft
Sc	Schmidt number, $(\mu_m/D_V\rho_m)$
T	temperature, ^{o}R
$T_{L,E}$	liquid equilibrium temperature, ^{o}R
t	time, sec
U	gas velocity, ft/sec
U_d	drop velocity, ft/sec
U_F	final gas velocity, ft/sec
ΔV	velocity difference between gas and drop, $U - U_d$, ft/sec
W	droplet weight, lb
x	distance downstream from injection, ft
x_{100}	distance required to vaporize a drop under 100-psia pressure and at specified conditions, ft
z	heat-transfer factor
ρ	density, lb/ft^3
μ	viscosity, lb/(ft)(sec)

Subscripts:

crit	critical value for liquid
G	gas value
L	liquid value
m	mean value based on film composition and/or temperature
o	initial value
T	gas value
v	vapor value

APPENDIX A

PROPERTY EQUATIONS FOR WATER VAPOR,

RANGE $1800^{\circ}\ R \leq T_m \leq 3800^{\circ}\ R$

$$C_{p,G} = -1.427\times10^{-8}\ T_m^2 + 1.4311\times10^{-4}\ T_m + 0.33575 + 235.67\left(P_T^{1.058}/T_m^{2.854}\right), \quad \text{Btu/(lb)(}^{\circ}\text{R)}$$

$$k_G = -4.03\times10^{-13}\ T_m^2 + 1.4674\times10^{-8}\ T_m - 6.729\times10^{-6}, \quad \text{Btu/(ft)(sec)(}^{\circ}\text{R)}$$

$$\mu_G = -7.95\times10^{-13}\ T_m^2 + 1.5559\times10^{-8}\ T_m - 1.5544\times10^{-6}, \quad \text{lb/(ft)(sec)}$$

$$D_V = (7.067\times10^{-7}\ T_m^2 + 2.0244\times10^{-3}\ T_m - 1.2285)/P_T, \quad \text{ft}^2\text{/sec}$$

APPENDIX B

CONDITIONS CAUSING DROPLET CRITICAL HEATING

Examination of equations (1) and (5) and consideration of the physical process causing thermal equilibrium explain the results of figure 1. The three most important parameters in determining the equilibrium temperature are the heat of vaporization H_V, and the vapor pressure P_L and total pressure P_T contained in $\ln\left(\frac{P_T}{P_T - P_L}\right)$. As the liquid temperature T_L increases, H_V decreases, and P_L and $\ln\left(\frac{P_T}{P_T - P_L}\right)$ increase. For a constant pressure and velocity flow field around the droplet, the mass-transfer rate dW/dt is roughly proportional to $\ln\left(\frac{P_T}{P_T - P_L}\right)$ with K as a proportionality factor. The enthalpy transferred away from the drop surface is proportional to the product of H_V and dw/dt.

Consider three cases: (I) $P_T \leq P_L$, (II) $P_L < P_T \leq P_{crit}$, and (III) $P_L \leq P_{crit} < P_T$. Case I corresponds to flash vaporization. The equations of this paper do not describe this process. The general history of a droplet for cases II and III are illustrated in figure 6. For simplicity, a constant incident heat flux to the droplet surface Q_{IN} was assumed. In case II, the droplet temperature rises to the steady-state temperature $T_{L,E}$, where $Q_{IN} = Q_{OUT} = H_V\,(dW/dt)$. Since $P_T \leq P_{crit}$, P_L can approach P_T as close as necessary to give a very high value of $\ln\left(\frac{P_T}{P_T - P_L}\right)$ and, correspondingly, a very high mass-transfer rate. Then Q_{OUT} may also become as large as necessary to equal Q_{IN}, and an equilibrium temperature is thus always assured.

In case III, however, $P_T > P_{crit}$ and the mass-transfer rate has an

upper limit defined by $\ln\left(\frac{P_T}{P_T - P_{crit}}\right)$ at $T_L = T_{crit}$. Since the heat of vaporization H_V goes to zero at this point, the quantity Q_{OUT} reaches a maximum at a short distance below T_{crit} then decreases to zero at T_{crit}. If $Q_{OUT} = Q_{IN}$ before this maximum occurs (curve (a)), an equilibrium temperature exists. If the maximum of Q_{OUT} is exactly equal to Q_{IN} (curve (b)), the equilibrium temperature which is the highest obtainable, occurs at the maximum. If the maximum of Q_{OUT} is less than Q_{IN} (curve (c)), the droplet continues heating the critical point. As P_T increases, curve (a) is shifted toward curve (c).

The preceding simplified model grossly describes the behavior of droplet equilibrium temperatures. However, the physical properties, the flow field surrounding the drop, and the gas temperature can also have an effect on steady-state temperature, as indicated in equations (1) and (5). For heptane, the property group $\left(\frac{C_{p,v} D_v M_L}{k_m R}\right)$ contained in z in equation (5) varies in value from 0.22 to 2.2, and the gradient of vapor pressure with liquid temperature is not very steep compared to oxygen. As a result, small changes in T_L do not cause large changes in $\ln\left(\frac{P_T}{P_T - P_L}\right)$. Coupled with an appreciable heat of vaporization (12 to 30 Btu/lb) in the region 1° to 10° F below the critical point, this causes the maximum Q_{OUT}, and hence the equilibrium temperature, to occur about 7° R below the critical temperature. It also allows other parameters to affect the solution. The influence of Nusselt number is indicated by the family of curves for heptane in figure 1. An increase in total gas temperature from 4000° to 6000° R causes a maximum increase of about 9° R in steady-state temperature and a 12-psi decrease in the total pressure required to reach the critical point.

In contrast, oxygen has a range in $\left(\frac{C_{p,v}\, D_v M_L}{k_m R}\right)$ from 0.01 to 0.16, a smaller heat of vaporization (2 to 15 Btu/lb) in the region 1° to 10° R below the critical temperature, and a very steep gradient of vapor pressure with liquid temperature. Thus, the steady-state temperature solution occurs where $\ln\left(\frac{P_T}{P_T - P_L}\right)$ is large and is changing rapidly with small changes in vapor pressure. This eliminates any effect of Nusselt number, and one curve of equilibrium temperatures satisfies all values of $r\,\Delta V$ with solutions still existing very close to the critical temperature of the liquid. This behavior is exhibited by oxygen in figure 1. Oxygen also shows only a tenth of a degree difference in equilibrium temperature when gas temperature is varied from 4000° to 6000° R.

REFERENCES

1. Priem, R. J., Propellant Vaporization as a Criterion for Rocket-Engine Design; Calculations Using Various Log-Probability Distributions of Heptane Drops. NACA TN 4098, (1957).

2. El Wakil, M. M., Uyehara, O. A., and Myers, P. S., A Theoretical Investigation of the Heating-Up Period of Injected Fuel Droplets Vaporizing in Air. NACA Tn 3179, (1954).

3. El Wakil, M. M., Priem, R. J., Brikowski, H. J., Myers, P. S., and Uyehara, O. A., Experimental and Calculated Temperature and Mass Histories of Vaporizing Fuel Drops. NACA TN 3490, (1956).

4. Priem, R. J., Vaporization of Fuel Drops Including the Heating-Up Period. Ph.D Thesis, Univ. Wisconsin, (1955).

5. Priem, R. J., Borman, G. L., El Wakil, M. M., Uyehara, O. A., and Myers, P. S., Experimental and Calculated Histories of Vaporizing Fuel Drops. NACA TN 3988, (1957).

6. Priem, R. J., and Heidmann, M. F., Propellant Vaporization as a Design Criterion for Rocket-Engine Combustion Chambers. NASA TR R-67, (1960).

7. Lambiris, S., and Combs, L. P., Steady-State Combustion Measurements in a LOX/RP-1 Rocket Chamber and Related Spray Analysis. Preprint 61-132-1820, Presented at IAS-ARS Meeting, Los Angeles, June 13-16 (1961).

8. Maxwell, J. B., Data Book on Hydrocarbons. (D. Van Nostrand Co., Inc., 1950), Chap. 4, p. 33; Chap. 7, pp. 94-95; Chap. 8, p. 140.

9. Baly, E. C. C., and Donnan, F. G., "The Variation with Temperature of the Surface Energies and Densities of Liquid Oxygen, Nitrogen, Argon, and Carbon Monoxide," J. Chem. Soc. (London), Trans. 81 (1902).

10. Division of Chemical Engineering, Liquid Propellants Handbook. Battelle Memorial Inst., Columbus 1, Ohio. (Contract NOa(S) 54-597-C, Dept. Navy, Bur. Aero. (S1-531), Wash. 25, D.C., Oct. 31 (1955).

11. Mathias, E., and Onnes, H. K., "The Rectelinear Diameter of Oxygen," Annales de Physique, 17, (1922). (Abs. from Chem. Abs., 16, 1922).

12. Woolley, H. W., Thermodynamic Properties of Molecular Oxygen. Rep. 2611, U.S. Dept. Commerce, Nat. Bur. Standards, Wash. D.C., June 30 (1953).

13. Kanarek, I. A., Properties of Handling and Storage Characteristics of Ethyl Alcohol and Liquid Oxygen. North Am. Aviation, Inc., Nov. 1 (1948).

14. Hirschfelder, J. O., Curtiss, C. F., and Bird, R. B., Molecular Theory of Gases and Liquids. (John Wiley & Sons, Inc. 1954).

15. Monchick, L., and Mason, E. A., "Transport Properties of Polar Gases," J. Chem. Phys., 35, no. 5, pp. 1676-1697 (1961).

16. Timrot, D. L., and Vargaftck, N. B.,"The Thermal Conductivity and Viscosity of Steam at High Temperatures and Pressures," J. Phys., U.S.S.R., II, pp. 101-111 (1940).

17. Keyes, F. G., "Viscosity and Heat Conduction of Steam," J. Am. Chem. Soc., 72, pp. 433-C (1950).

18. Myers, P. S., Personal Communication. Univ. Wisconsin, (1962).

19. Hall, A. R., Experimental Temperature Gradients in Burning Drops. Seventh Symposium (International) on Combustion, Butterworths Sci. Pub. (London), 641-648. (1958).

FIGURE LEGENDS

Figure 1. - Effect of total pressure on reduced droplet equilibrium temperature for heptane and oxygen droplets. Gas temperature, 5000° R.

(a) Reduced temperature and evaporation rate.

(b) Weight ratio and radius.

Figure 2. - Heptane droplet history. Initial droplet radius, 3.2808×10^{-4} ft (100 microns); gas pressure, 1000 psia; gas temperature, 5000° R; final gas velocity, 800 ft/sec; droplet injection velocity, 80 ft/sec; droplet injection temperature, 650° R.

(a) Reduced temperature and evaporation rate.

(b) Weight ratio and radius.

Figure 3. - Oxygen droplet history. Initial droplet radius, 3.2808×10^{-4} ft (100 microns); gas pressure, 1000 psia; gas temperature, 5000° R; final gas velocity, 800 ft/sec; droplet injection velocity, 80 ft/sec; droplet injection temperature, 140° R.

Figure 4. - Normalized vaporization length of heptane and oxygen droplets. Final gas velocity, 800 ft/sec; gas temperature, 5000° R; initial droplet velocity, 80 ft/sec; initial droplet temperature: heptane, 650° R; oxygen, 140° R.

Figure 5. - Percent weight vaporized before the critical point is reached for heptane and oxygen droplets. Final gas velocity, 800 ft/sec; gas temperature, 5000° R; initial droplet velocity, 80 ft/sec; initial droplet temperatures: heptane, 650° R; oxygen 140° R.

Figure 6. - Variation of droplet heat and mass-transfer rates (Q_{IN}, Q_{OUT}, dW/dt) and heat of vaporization (H_V) with liquid temperature, T_L.

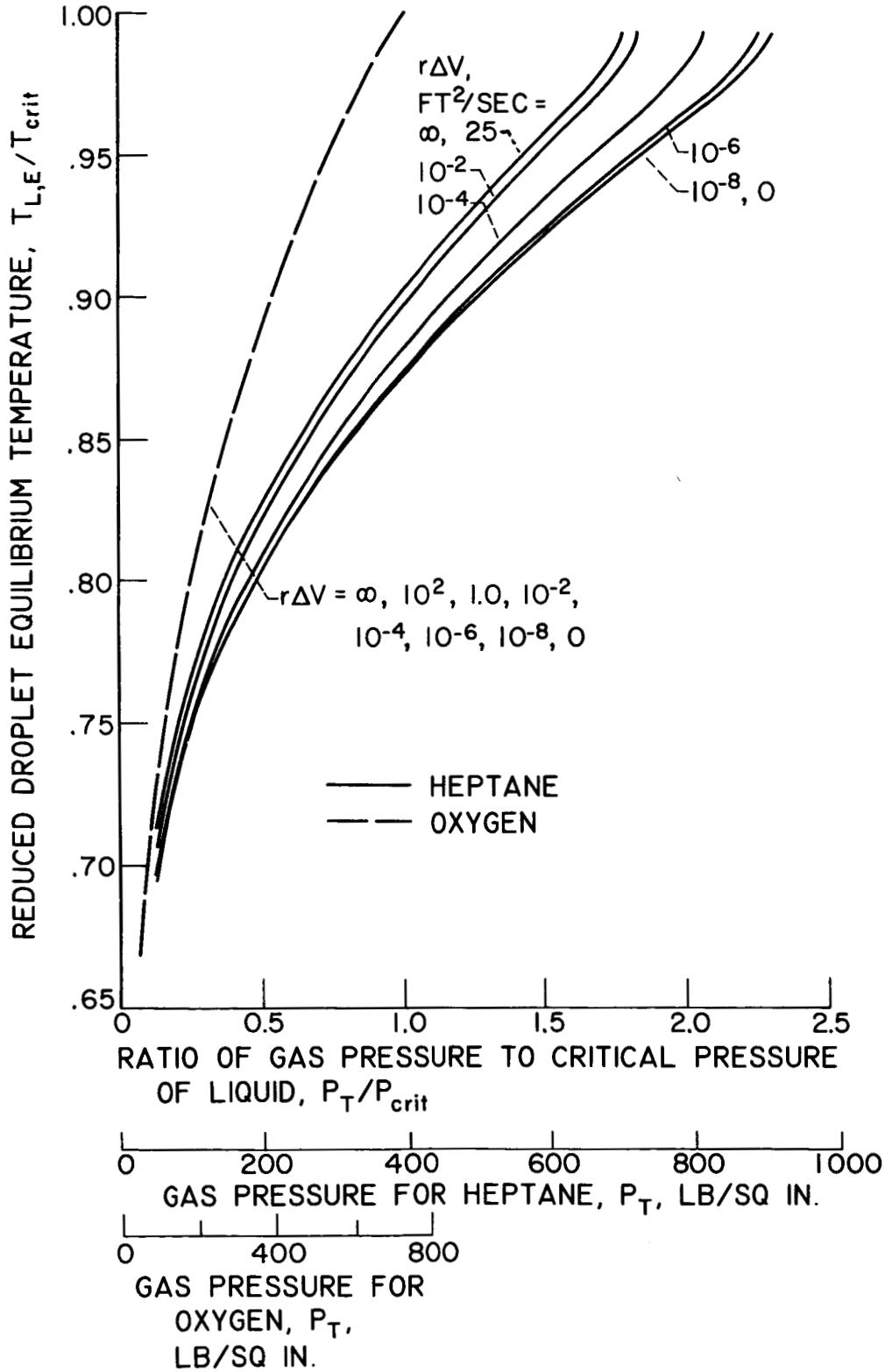

Figure 1. - Effect of total pressure on reduced droplet equilibrium temperature for heptane and oxygen droplets. Gas temperature, 5000° R.

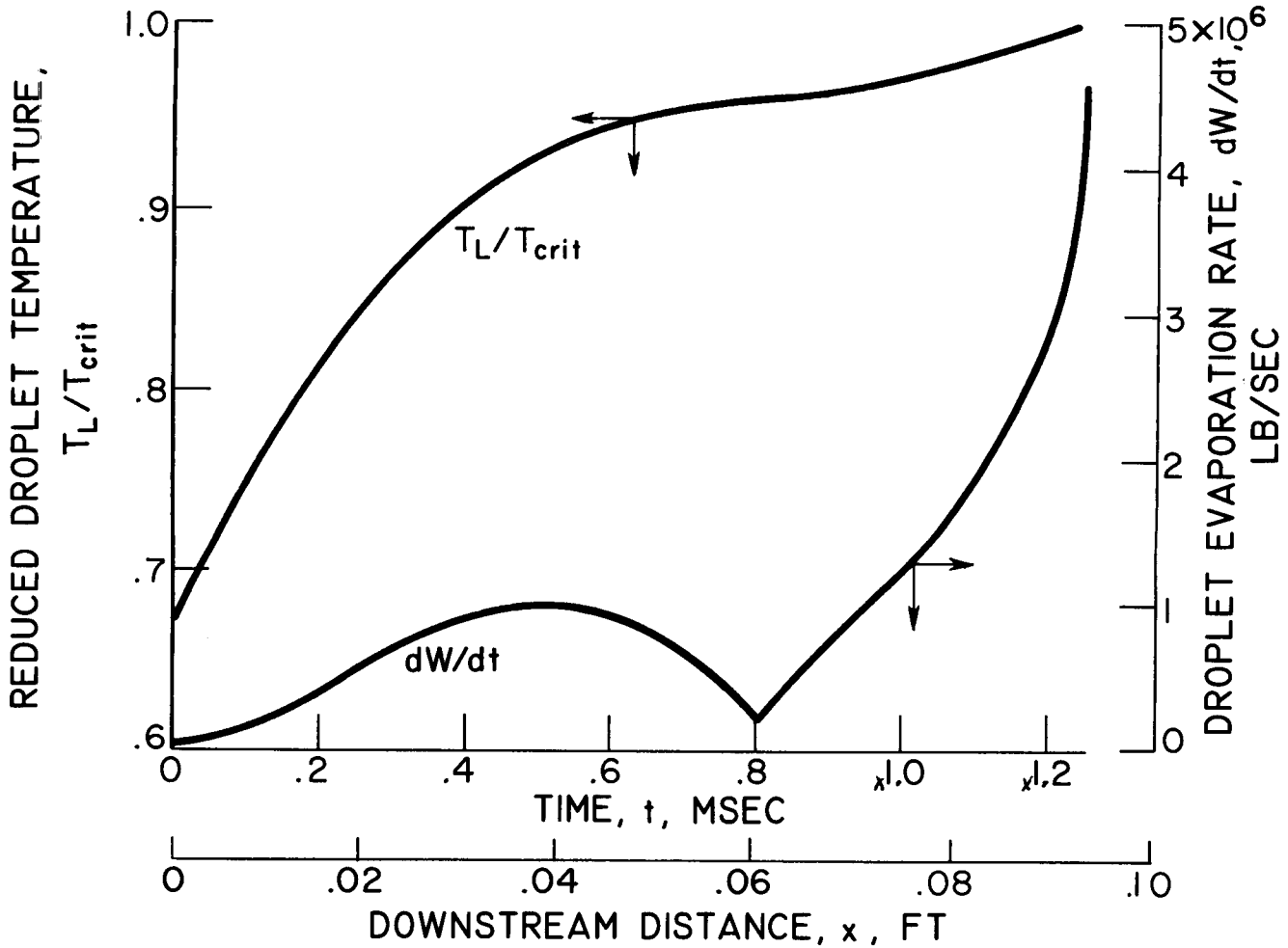

(a) Reduced temperature and evaporation rate.

Figure 2. - Heptane droplet history. Initial droplet radius, 3.2808×10^{-4} ft (100 microns); gas pressure, 1000 psia; gas temperature, 5000° R; final gas velocity, 800 ft/sec; droplet injection velocity, 80 ft/sec; droplet injection temperature, 650° R.

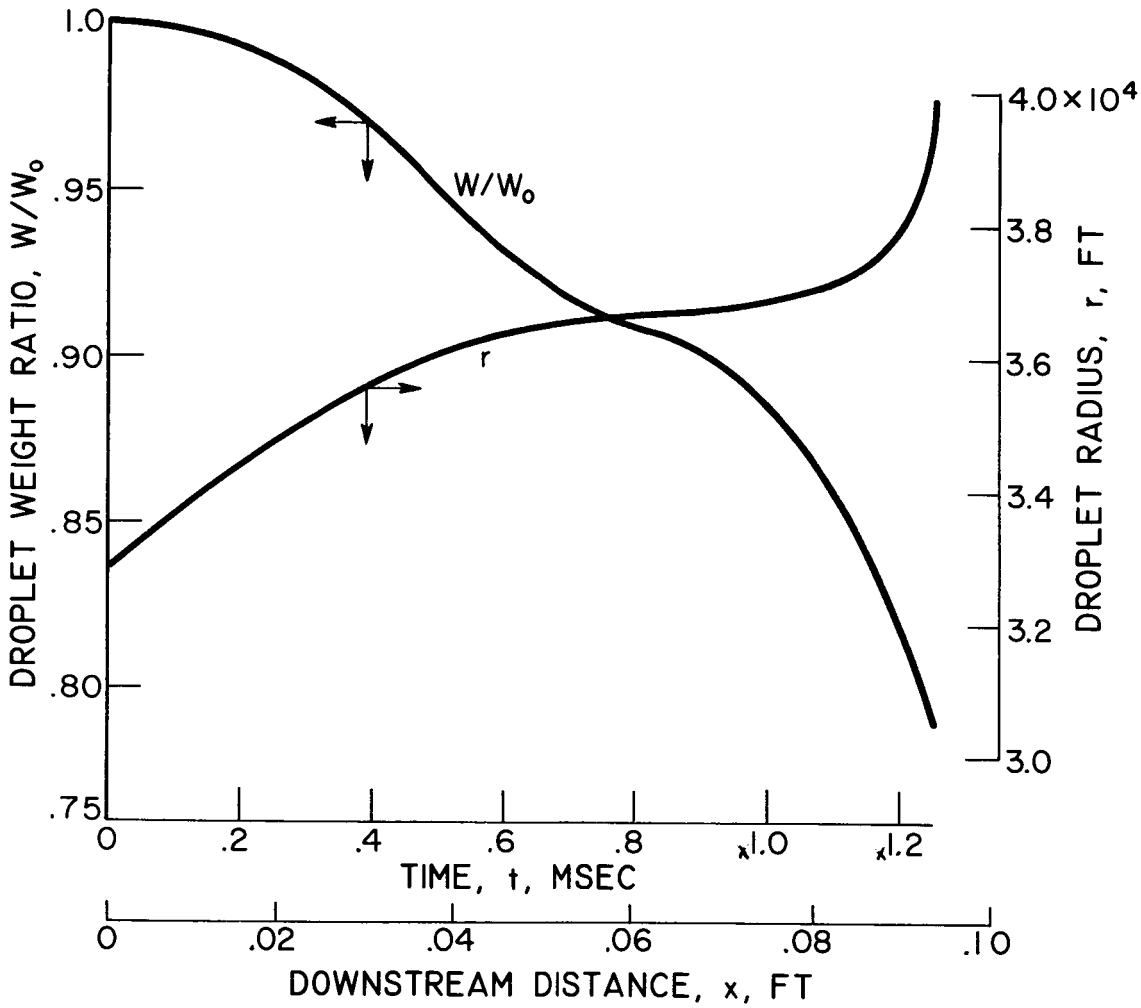

(b) Weight ratio and radius.

Figure 2. - Concluded. - Heptane droplet history. Initial droplet radius, 3.2808×10^{-4} ft (100 microns); gas pressure, 1000 psia; gas temperature, 5000° R; final gas velocity, 800 ft/sec; droplet injection velocity, 80 ft/sec; droplet injection temperature, 650° R.

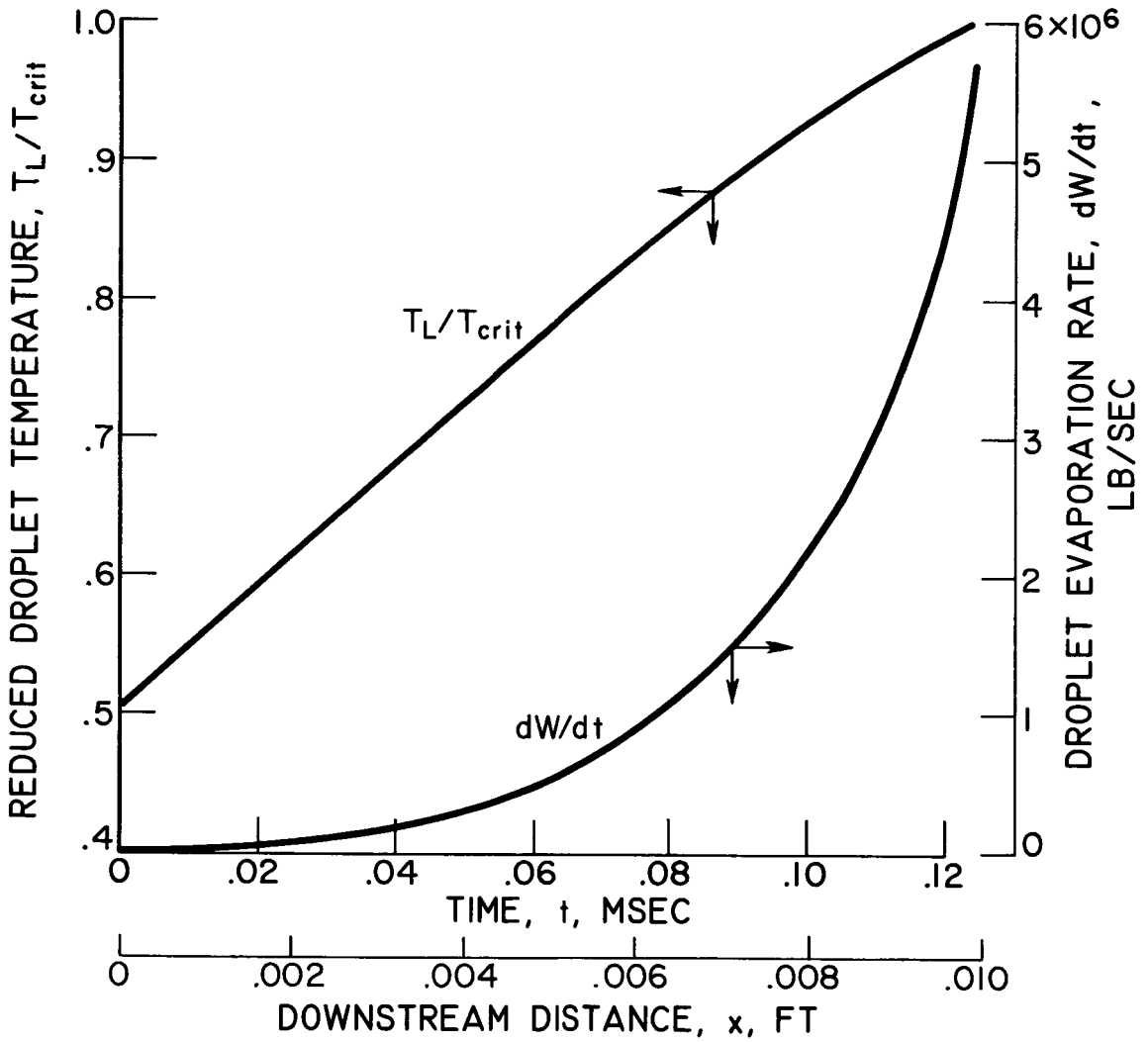

(a) Reduced temperature and evaporation rate.

Figure 3. - Oxygen droplet history. Initial droplet radius, 3.2808×10^{-4} ft (100 microns); gas pressure, 1000 psia; gas temperature, 5000° R; final gas velocity, 800 ft/sec; droplet injection velocity, 80 ft/sec; droplet injection temperature, 140° R.

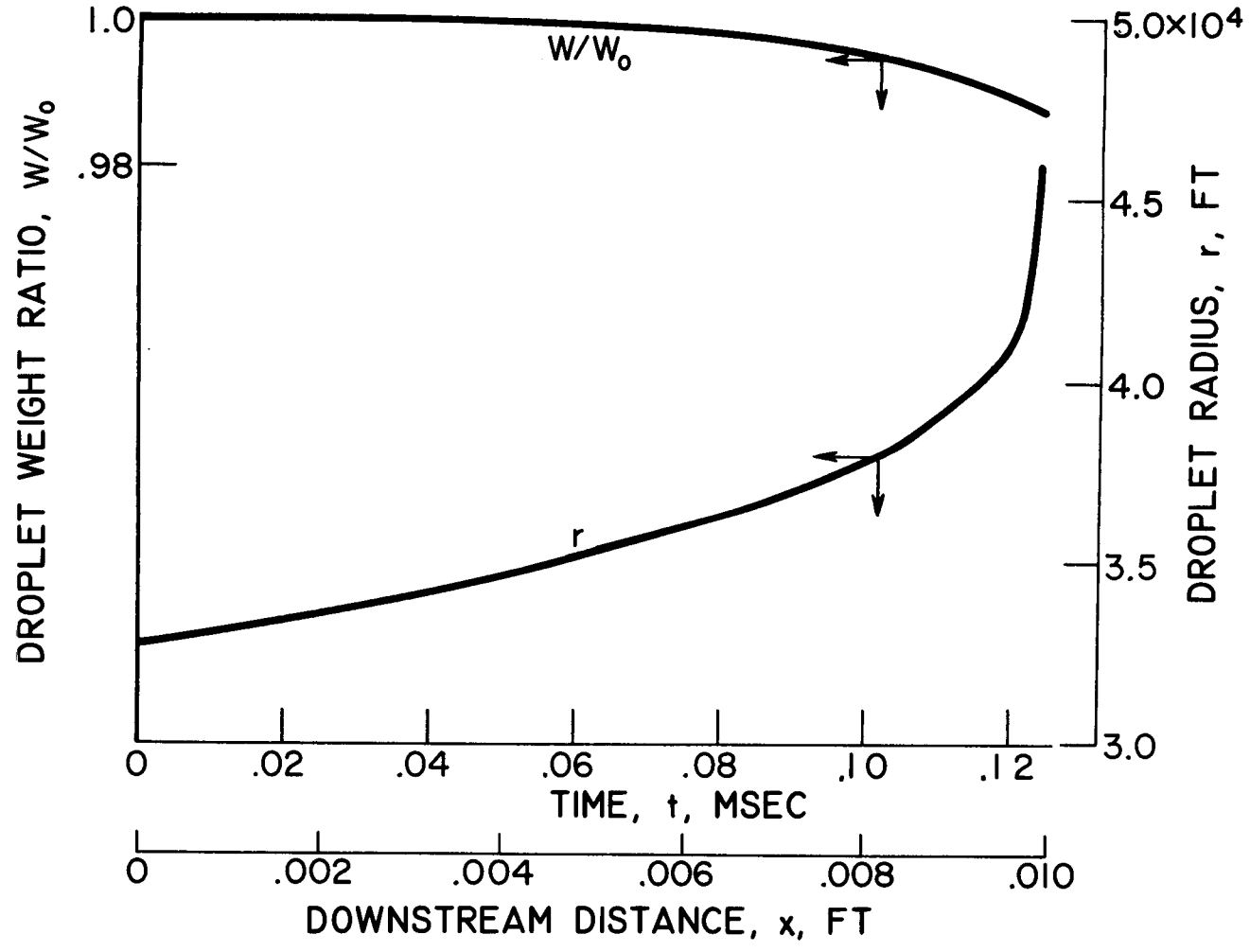

(b) Weight ratio and radius.

Figure 3. - Concluded. - Oxygen droplet history. Initial droplet radius, 3.2808×10^{-4} ft (100 microns); gas pressure, 1000 psia; gas temperature, 5000° R; final gas velocity, 800 ft/sec; droplet injection velocity, 80 ft/sec; droplet injection temperature, 140° R.

E-1973

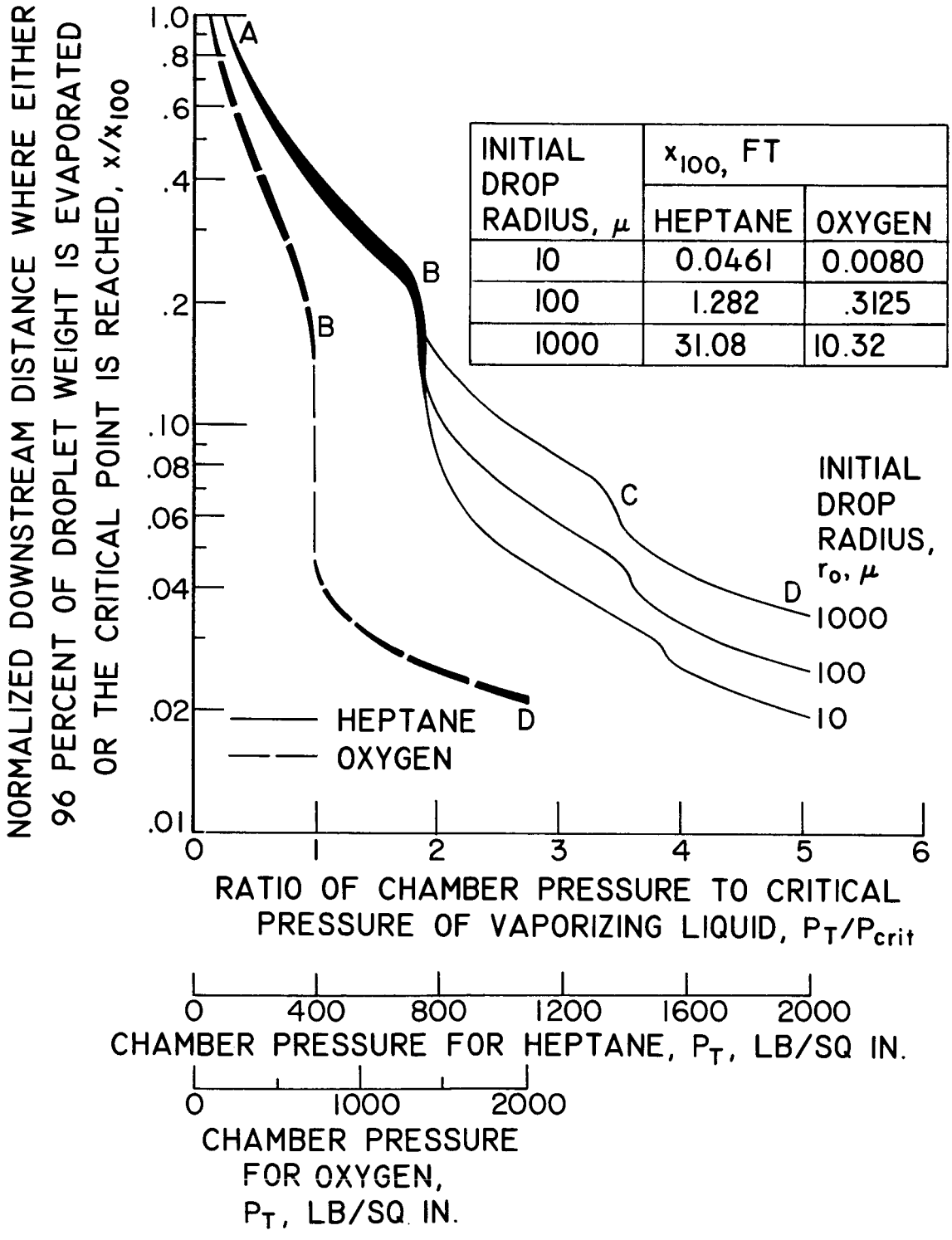

INITIAL DROP RADIUS, μ	x_{100}, FT	
	HEPTANE	OXYGEN
10	0.0461	0.0080
100	1.282	.3125
1000	31.08	10.32

Figure 4. - Normalized vaporization length of heptane and oxygen droplets. Final gas velocity, 800 ft/sec; gas temperature, 5000° R; initial droplet velocity, 80 ft/sec; initial droplet temperatures: heptane, 650° R; oxygen, 140° R.

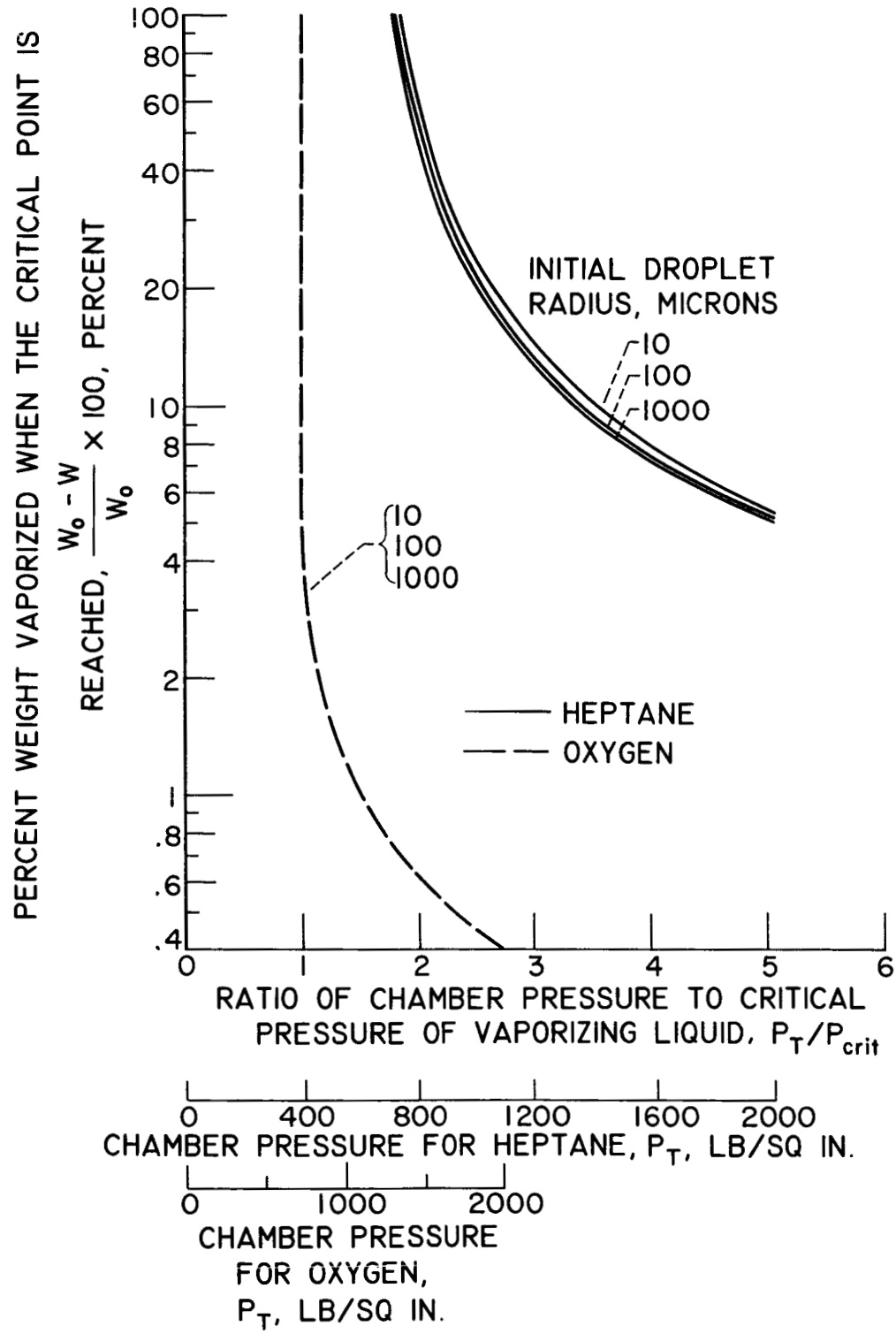

Figure 5. - Percent weight vaporized before the critical point is reached for heptane and oxygen droplets. Final gas velocity, 800 ft/sec; gas temperature, 5000° R; initial droplet velocity, 80 ft/sec; initial droplet temperatures: heptane, 650° R; oxygen, 140° R.

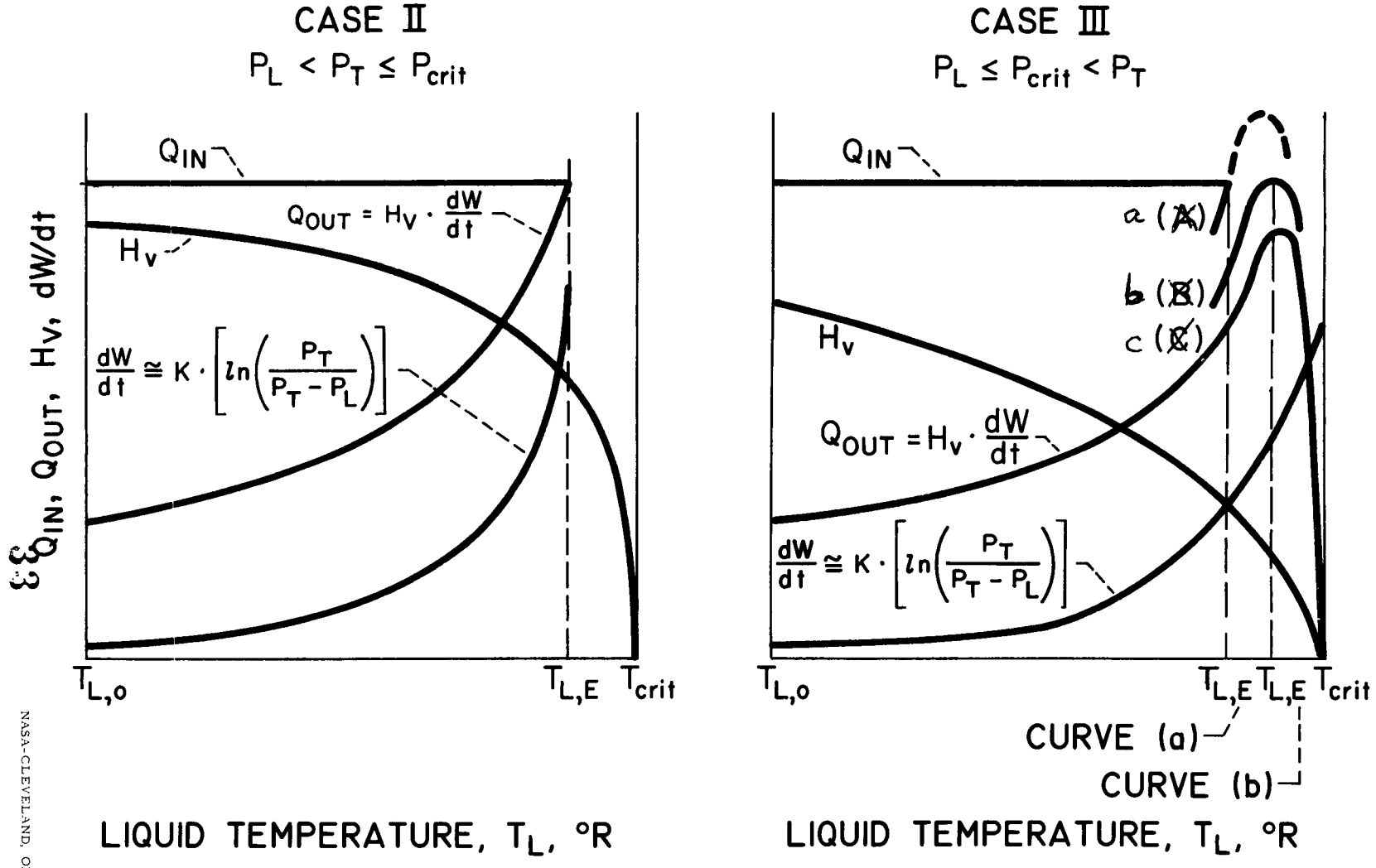

Figure 6. - Variation of droplet heat and mass-transfer rates (Q_{in}, Q_{out}, dW/dt) and heat of vaporization (H_v) with liquid temperature, T_L.